In Vitro Evaluation and Mitigation of Niclosamide's Liabilities as a COVID-19 Treatment.

Jesse W. Wotring[1], Sean M. McCarty[1], Khadija Shafiq[1], Charles J. Zhang[1], Theophilus Nguyen[2], Sophia R. Meyer[1], Reid Fursmidt[2], Carmen Mirabelli[3], Martin C. Clasby[1], Christiane E. Wobus[3], Matthew J. O'Meara[4], Jonathan Z. Sexton[1,2,5] *

[1] Department of Medicinal Chemistry, College of Pharmacy, University of Michigan, Ann Arbor, MI, 48109, USA.

[2]Department of Internal Medicine, Gastroenterology and Hepatology, Michigan Medicine at the University of Michigan, Ann Arbor, MI, 48109, USA.

[3]Department of Microbiology and Immunology, University of Michigan, Ann Arbor, MI, USA.

[4]Department of Computational Medicine and Bioinformatics, University of Michigan, Ann Arbor, MI 48109, USA.

[5]U-M Center for Drug Repurposing, University of Michigan, Ann Arbor, MI, 48109, USA.

* Corresponding author: jzsexton@med.umich.edu

Abstract

Niclosamide, an FDA-approved oral anthelmintic drug, has broad biological activity including anticancer, antibacterial, and antiviral properties. Niclosamide has also been identified as a potent inhibitor of SARS-CoV-2 infection *in vitro,* generating interest in its use for the treatment or prevention of COVID-19. Unfortunately, there are several potential issues with using niclosamide for COVID-19, including low bioavailability, significant polypharmacology, high cellular toxicity, and unknown efficacy against emerging SARS-CoV-2 variants of concern. In this study, we used high-content imaging-based immunofluorescence assays in two different cell models to assess these limitations and evaluate the potential for using niclosamide as a COVID-19 antiviral. We show that despite promising preliminary reports, the antiviral efficacy of niclosamide overlaps with its cytotoxicity giving it a poor *in vitro* selectivity index for anti-SARS-CoV-2 inhibition. We also show that niclosamide has significantly variable potency against the different SARS-CoV-2 variants of concern and is most potent against variants with enhanced cell-to-cell spread including B.1.1.7. Finally, we report the activity of 33 niclosamide analogs, several of which have reduced cytotoxicity and increased potency relative to niclosamide. A preliminary structure-activity relationship analysis reveals dependence on a protonophore for antiviral efficacy, which implicates nonspecific endolysosomal neutralization as a dominant mechanism of action. Further single-cell morphological profiling suggests niclosamide also inhibits viral entry and cell-to-cell spread by syncytia. Altogether, our results suggest that niclosamide is not an ideal candidate for the treatment of COVID-19, but that there is potential for developing improved analogs with higher clinical translational potential in the future.

Key Words: Niclosamide, SARS-CoV-2, COVID-19, Polypharmacology, Drug Repurposing

53 **Introduction**

54 Since it emerged as a novel betacoronavirus in late 2019, Severe Acute Respiratory Syndrome
55 Coronavirus 2 (SARS-CoV-2) has caused a global pandemic[1]. COVID-19, the disease caused by
56 SARS-CoV-2 infection, presents as varying symptoms with different degrees of severity ranging
57 from dry cough and difficulty breathing to acute cardiac injury and refractory pulmonary
58 failure[2,3]. As of April 2022, COVID-19 has caused the death of over six million individuals
59 worldwide[4] and this death toll continues to increase as new SARS-CoV-2 Variants of Concern
60 (VOCs) emerge with enhanced transmissibility and increased adaptive immune escape[5].

61 The deadly impact of COVID-19 has created a need to identify potential antiviral treatments for
62 SARS-CoV-2 infection. This has culminated in the development and FDA-
63 authorization/approval of several vaccines[6], and three small-molecule antiviral medications
64 including remdesivir[7], molnupiravir[8], and Paxlovid[9]. Unfortunately, because of limited
65 worldwide vaccine availability[10], the modest clinical efficacy of existing antivirals[8,9,11,12], and the
66 potential resistance of SARS-CoV-2 variants[13,14], additional therapeutics are urgently needed to
67 help stop the spread of the virus.

68 A promising strategy for identifying new therapies with the potential for rapid deployment is
69 drug repurposing, whereby compounds with already established safety profiles and robust supply
70 chains are used to treat other diseases[15]. Since the start of the pandemic, several large-scale drug
71 repurposing screens have been conducted[16–20] and have identified many different potential
72 candidates for the treatment of COVID-19. One of the repurposed drugs, which had potent anti-
73 SARS-CoV-2 efficacy *in vitro,* was the oral anthelmintic compound niclosamide[17,20].

74 Traditionally used to treat tapeworm infection, niclosamide has been often repurposed in treating
75 a wide range of diseases including several cancers, bacterial infections, viral infections, type 2
76 diabetes, non-alcoholic fatty liver disease, and rheumatoid arthritis[21]. This range of potential uses
77 is due to the significant polypharmacology of niclosamide, which is known to act on many
78 different biological targets and is a modulator of the Wnt/b-catenin, mTOR and JAK/STAT3
79 signaling pathways among others[21]. Niclosamide is also a weakly acidic lipophilic protonophore
80 that can disrupt pH gradients by shuttling protons across lipid membranes[22] including
81 mitochondria and lysosomes/endosomes. This physiochemical property is responsible for its
82 activity as a mitochondrial uncoupler[23] and contributes to its broad activity against viruses, many
83 of which rely on endosomal-cytoplasmic pH gradients in their life cycle[24].

84 Niclosamide was also previously identified as a potential antiviral for the related coronavirus
85 SARS-CoV, where it was shown to inhibit viral replication *in vitro* with low micromolar
86 potency[25]. The mechanism of action (MOA) for niclosamide against SARS-CoV-2 may be more
87 complex and multimodal than for SARS-CoV. Niclosamide has been shown to inhibit SARS-
88 CoV-2 endocytosis mediated entry[26], block viral replication by promoting cellular autophagy[27],
89 and disrupt spike (S) protein-mediated syncytia formation via inhibition of the host cell calcium-
90 dependent scramblase TMEM16F[28]. Given the polypharmacology of niclosamide, it is likely that
91 there are additional factors that contribute to its overall efficacy and complicate its MOA. The
92 degree to which each of these MOAs plays a role in the antiviral efficacy of niclosamide against
93 SARS-CoV-2 is unclear.

94 While niclosamide was clinically effective as an anthelmintic drug, it has substantial limitations
95 for use as a COVID-19 antiviral including its low oral bioavailability (<10%) and poor water
96 solubility[29,30]. Oral administration of niclosamide at 5 mg/kg in rats reaches a maximal serum

97 concentration (C_{max}) of only 354 ± 152 ng/mL[31]. As a result, the concentration of niclosamide in
98 the lungs would likely be too low to achieve therapeutic effect. Another limitation exists in that
99 polypharmacology is generally associated with increased adverse effects for repurposed drugs[32].
100 Finally, the toxicity of niclosamide is a major concern as it has been previously repurposed as a
101 broad anti-cancer agent and has shown significant cytotoxic/cytostatic effects *in vitro*[33,34]. A
102 better understanding of the anti-SARS-CoV-2 mechanism of action for niclosamide, including
103 potential toxicity and activity against emerging variants of concern (VOC), is needed to
104 effectively evaluate its clinical potential.

105 The goal of this study was to expand upon the understanding of niclosamide anti-SARS-CoV-2
106 activity and its potential as a clinical therapeutic using high content fluorescence imaging and
107 analysis. Herein, we reveal some of the mechanistic and cell morphological characteristics of
108 niclosamide activity, including an analysis of its cellular toxicity after long-term exposure to a
109 therapeutic antiviral dose. Additionally, we investigate niclosamide antiviral activity against
110 SARS-CoV-2 viral VOCs. We hypothesized that because the fusogenicity amongst SARS-CoV-
111 2 variants is known to be different[35–37], the potency/efficacy of niclosamide may also vary
112 between strains. Here we reveal the potency of niclosamide against several variants including
113 WA1 (wildtype), B.1.1.7 (alpha), B.1.351 (beta), P.1 (gamma) and B.1.617.2 (delta). Lastly, we
114 report the *in vitro* results of a structure-activity relationship (SAR) campaign of 33 niclosamide
115 analogs against SARS-CoV-2 in two different cell lines (VeroE6 and H1437). We used the
116 results from this SAR campaign to reveal additional mechanistic details for niclosamide, and aid
117 with the identification of structural analogs with reduced cellular toxicity. Altogether, our results
118 suggest that niclosamide itself is not a suitable candidate for the treatment of COVID-19, yet
119 there is potential for developing analogs with improved properties for future clinical use.

120 **Results**

121 **Niclosamide has a poor selectivity index**

122 One major concern regarding the utility of niclosamide as a COVID-19 antiviral is its
123 cytotoxicity in comparison with its antiviral efficacy. Here, we aimed to determine the selectivity
124 index (SI) of niclosamide *in vitro* against SARS-CoV-2 in two different cell models for
125 infection, VeroE6 and the human lung adenocarcinoma cell line H1437. To assess compound-
126 related toxicity, we evaluated the effects of niclosamide on cells after 72 hours of compound
127 exposure. We designed and optimized two separate high-content fluorescence imaging assays in
128 384-well plate format using the different cell lines and measured cell viability and viral
129 inhibition concurrently. In both assays, we used the detection of viral nucleocapsid (N) protein as
130 a direct marker for SARS-CoV-2 infection and cell count per well as an indicator of cell
131 viability. As summarized in the **Figure 1A** workflow, VeroE6 or H1437 cells were preincubated
132 with a 10-point 2-fold dilution series of niclosamide (N=10 replicates per condition) for 24 hours
133 and then infected with the SARS-CoV-2 B.1.1.7 variant for an additional 48 hours post-infection
134 (p.i.). Following infection, cells were fixed, permeabilized, and stained to identify nuclei and
135 viral N protein. Assay plates were imaged at 10X magnification using a CX5 high content
136 imaging platform (N=9 fields captured per well) and processed using the image segmentation
137 and analysis software CellProfiler. Data from the CellProfiler output were used to determine
138 percent infection and percent viability. Infection data were normalized to the average well-level
139 % N positive for infected controls (mock) in each cell line (**Supplementary Figure S1A**).
140 Percent viability was determined by normalizing the average well-level cell counts for the
141 infected control (**Supplementary Figure S1B**). We found that niclosamide has potent 50%
142 maximal inhibition (IC_{50}) values of 564 nM for VeroE6 and 261 nM for H1437. However,

143 niclosamide caused a 50% reduction in cell viability (CC_{50}) at concentrations of 1050 nM and
144 438 nM for VeroE6 and H1437, respectively, resulting in poor selectivity indices in both cell
145 lines (1.86 for VeroE6 and 1.67 for H1437). The concentration-response curves for this
146 experiment are shown in **Figure 1B** along with representative images for infected control, mock,
147 and 10 μM niclosamide conditions for each cell line. As illustrated in **Figure 2B** and
148 Supplementary **Figure 1A**, the average percentage of N protein-positive cells in untreated
149 infected controls after 48 hours of infection was significantly higher in VeroE6 (69 %) than
150 H1437 (9%) indicating more efficient cell-to-cell spread in the former. In conclusion,
151 niclosamide has a low SI in two cell lines of fibroblast origin, representing a liability for
152 therapeutic use.

153 **Niclosamide potency is SARS-CoV-2 variant dependent**

154 Niclosamide has a complex polypharmacology profile against host-cell pathways, which may
155 contribute to the antiviral efficacy and/or cytotoxicity of the compound and lead to variable
156 responses across SARS-CoV-2 VOCs that rely differentially on these pathways. To evaluate the
157 antiviral efficacy of niclosamide against VOCs, we used a modified infection assay in VeroE6.
158 Exposure to niclosamide was reduced to a 1- hour preincubation and the assay window was
159 shortened to 24 hours post-infection (**Figure 2A**) to limit compound toxicity. VeroE6 cells were
160 used as they demonstrated a higher N-protein positivity rate than H1437 cells. We evaluated the
161 antiviral activity of niclosamide against the WA1 (wildtype), B.1.1.7 (alpha), B.1.351 (beta), P.1
162 (gamma), and B.1.617.2 (delta) variants in 10-point, 2-fold dilution. 10-Point dose-response
163 efficacy experiments showed niclosamide had statistically significant differences in efficacy
164 against VOCs, was most potent against the B.1.1.7 strain (IC_{50} = 298 nM), and least potent
165 against the WA1 strain (IC_{50} = 1664 nM). The full efficacy data for all variants are shown in

166 **Figures 2B-C**. The CC_{50} for niclosamide in this shortened assay was > 10 μM (not shown).
167 These data demonstrate variant dependent antiviral efficacy of niclosamide.

168 **High-content analysis suggests inhibition of entry and syncytia formation**

169 Cell morphologic analysis of cells infected with VOCs, under the treatment of niclosamide,
170 revealed several defining characteristics of infection influenced by compound treatment. We
171 quantified these observations using morphological cell profiling analysis. We used data (B.1.1.7
172 variant in VeroE6) from the viral control (mock) and three different efficacious concentrations of
173 niclosamide around its IC_{50} (156 nM, 313 nM, 625 nM) to reanalyze using a more extensive
174 analysis pipeline that included intensity and area/shape measurements for both nuclear and viral
175 channels. For this analysis, syncytia/individually infected cells were defined as "viral objects."
176 We determined that treatment with niclosamide decreased the maximum size of syncytia (**Figure**
177 **3A**) consistent with an inhibition of cell-to-cell spread. We also found that treatment reduced the
178 number of individually infected cells within a well (**Figure 3B**) consistent with an inhibition of
179 viral entry. Finally, we found that the N protein intensity of remaining viral objects increased
180 with escalating concentrations of niclosamide (**Figure 3C**). The combination of these
181 observations suggests multiple MOA including inhibition of viral entry and cell-to-cell spread
182 resulting in fewer infected cells with dramatically increased cellular viral N protein content.
183 These results provide support for the polypharmacology of niclosamide that contributes to
184 multimodal efficacy against SARS-CoV-2. In addition, these results suggest that niclosamide
185 may not directly inhibit viral replication *in vitro*.

186

187

188 **Structure-activity relationship of niclosamide analogs versus SARS-CoV-2 infection**

189 Efficacy and cytotoxicity of 33 previously designed analogs[38] of niclosamide were used to
190 establish a preliminary structure-activity relationship (SAR) profile for niclosamide for anti-
191 SARS-CoV-2 activity in VeroE6 and H1437 cell lines. These analogs were also salicylanilides
192 and had substituent modifications on the nitroaniline and/or chlorosalicyl rings (**Figure 4A**)
193 intending to improve the selectivity while maintaining antiviral efficacy. Analog structures are
194 shown in **Supplementary Figure S2**. Analogs were evaluated using the assay described in
195 **Figure 1A**. All analogs were tested in 10-point 2-fold dilution series (N=3) from a starting
196 concentration of 20 μM. VeroE6 analog screening was performed using the B.1.1.7 variant at an
197 MOI of 0.1, while H1437 screening was performed using the WA1 variant at an MOI of 1. The
198 results from compound testing are summarized in **Table 1**, which includes IC_{50} and CC_{50} values
199 for both cell lines. As shown in Table 1, we found that 12 analogs retained IC_{50} values in the
200 nanomolar or micromolar range in VeroE6, while 8 compounds were efficacious in both VeroE6
201 and H1437. Four compounds (2, 7, 11, 24) showed improved potency and reduced cytotoxicity
202 against VeroE6 compared to niclosamide (**Figure 4C-F**). Overall, improvements in cytotoxicity
203 were less pronounced against H1437. Notably, the variant dependent potency difference was
204 conserved in H1437 cells and was significantly less potent against WA1 (IC_{50} = 16770 nM) than
205 B.1.1.7 (IC_{50} = 261 nM), consistent with results in VeroE6 cells.

206 In general, we found that the replacement of the nitro group on the nitroaniline ring was well
207 tolerated (compounds 5, 6, 7, 24 and 34) and improved the selectivity index. We also noted that
208 modification to the chloro position on the salicylic acid ring (R2) was well tolerated and all
209 compounds with only this modification retained antiviral efficacy (compounds 2, 3, 4, 11, 12).
210 Many analogs (compounds 7,8 12-19, 25, 28, 29, and 33) were found to exacerbate infection in

211 H1437 cells (**Supplementary Figure S3**) and showed inverted concentration-response curves at
212 high concentrations. Remarkably, the removal of the hydroxyl group (R1) on the salicylic acid
213 ring (compound 9) resulted in a complete loss of activity in both VeroE6 and H1437 (**Figure**
214 **5A**). This hydroxyl group has been previously reported as the protonophore responsible for the
215 mitochondrial uncoupling activity of niclosamide[23,38].

216 Given the drastic loss of activity, we evaluated the anti-SARS-CoV-2 efficacy of other
217 protonophore mitochondrial uncouplers including FCCP[39], 2,4 DNP[40], oxyclozanide[41] and
218 dicumarol[42]. These compounds were evaluated against WA1 and B.1.1.7 variants in VeroE6 cells
219 using the 24-hour infection conditions described in **Figure 3A**. Both FCCP and oxyclozanide
220 showed efficacy in the micromolar range (**Figure 5B-F)**. The potency of these compounds was
221 higher against B.1.1.7 than WA1, however the difference was more pronounced for niclosamide.
222 These results indicate that the mechanism of action for niclosamide against SARS-CoV-2 is at
223 least partially due to its physiochemical property as a protonophore, implicating energetic stress
224 response pathways in SARS-CoV-2 infection.

225 **Discussion**

226 There remains an urgent need for COVID-19 therapeutics, which can be used to prevent or treat
227 the spread of the virus SARS-CoV-2. The FDA approved oral anthelmintic drug niclosamide has
228 antiviral activity against SARS-CoV-2 infection *in vitro* and *in* vivo[43], which has generated
229 interest in its application for the treatment of COVID-19 and resulted in the conductance of
230 several human clinical trials. However, given its high cytotoxicity, unknown efficacy against
231 SARS-CoV-2 variants, low systemic bioavailability, and significant polypharmacology, we were
232 hesitant to consider niclosamide as a promising antiviral option. In this study, we used high-
233 content imaging of SARS-CoV-2 infected cells to evaluate some of the limitations of

234 niclosamide as a COVID-19 antiviral. We also extended our studies to structural analogs of
235 niclosamide, intending to reveal a preliminary structure-activity relationship profile that could be
236 used for future compound development.

237 Niclosamide has potent cytotoxic/cytostatic effects when applied directly to cells *in vitro*[34],
238 suggesting that it may have high acute toxicity *in vivo* with increased systemic exposure.
239 Clinically, the cytotoxicity is limited by the poor bioavailability of niclosamide, which has low
240 systemic exposure. To evaluate niclosamide toxicity, we used high-content fluorescence imaging
241 to determine a selectivity index for niclosamide in two different cell models including VeroE6
242 and the more physiologically relevant human lung adenocarcinoma cell line H1437. We found
243 that niclosamide has a very poor selectivity index in both cell lines (SI <2) after 72 hours of
244 compound exposure, suggesting that it would likely have a small therapeutic window clinically
245 even if the compound exposure was high enough in the lungs for antiviral efficacy. Longer
246 durations of exposure to niclosamide at relevant antiviral concentrations are likely to cause
247 significant side effects, which limits clinical application. Further studies are needed to evaluate
248 the safety of niclosamide at antiviral concentrations *in vivo*.

249 Our results are consistent with the results from recent clinical studies of niclosamide. Since it
250 was identified as an anti-SARS-CoV-2 agent *in vitro*, there have been several clinical studies to
251 evaluate the antiviral efficacy and safety of niclosamide. Notably, a recent phase 2 clinical trial
252 using 2g of orally administered niclosamide for 7 days revealed no statistically significant effect
253 on the duration of the contagious period of SARS-CoV-2[44]. While niclosamide was well
254 tolerated in this trial, the low efficacy and low adverse event rate are likely because the systemic
255 exposure is lower than what is required to observe antiviral activity or compound-related
256 toxicity. To address the poor oral bioavailability, several different formulations have been

257 developed for niclosamide to improve its exposure to the necessary site of action[45,46]. This has
258 included a formulation as an inhalable/intranasal powder to increase compound exposure in the
259 lungs. Unfortunately, a recent phase-1 safety trial using 50 mg over 2.5 days of
260 inhalable/intranasal niclosamide revealed moderate lung irritation in 59% of participants, which
261 suggests compound-related toxicity may be playing a significant role at higher local
262 concentrations in the lungs[47]. Although niclosamide is generally well-tolerated when used as an
263 anthelmintic drug, this is because it has low bioavailability, poor solubility, and stays within the
264 GI tract with very low systemic exposure.

265 A further limitation for using niclosamide as a COVID-19 therapeutic is its unknown efficacy
266 against the different emerging SARS-CoV-2 VOCs. We determined the efficacy for niclosamide
267 against the WA1 (wildtype), B.1.1.7 (alpha), B.1.351 (beta), P.1 (gamma) and B.1.617.2 (delta)
268 variants in VeroE6 cells. We found that there were significant differences in potency ranging
269 from 298 nM (beta variant) to 1664 nM (wildtype). Interestingly, the trend in potency correlates
270 with the ACE2 binding affinity for the different variants[48]. Variants, including alpha and beta,
271 also have higher fusogenicity than the wildtype variant and are more likely to undergo cell-to-
272 cell spread by syncytia[35], which may help explain the differences in potency.

273 These results are in contrast with those reported by Weiss *et al.*, which showed no significant
274 difference in potency amongst variants[49]. However, their study used qRT-PCR of viral RNA to
275 determine IC_{50} values, which is far less sensitive than a high-content imaging approach and does
276 not provide information on the clinically relevant endpoint of cell-to-cell spread inhibition.
277 Given the differences in potency amongst SARS-CoV-2 variants of concern, there arises a
278 concern for the rapid development or selection of resistant strains that do not respond to
279 niclosamide treatment. While the emergence of drug resistance is possible for any mechanism of

280 action inhibiting SARS-CoV-2, the pronounced difference between niclosamide's efficacy
281 amongst the VOCs makes niclosamide resistance inexorable. Further studies to understand the
282 mechanistic differences underlying variant-dependent responses to drugs like niclosamide may
283 ultimately inform *de novo* drug development for COVID-19.

284 To understand the MOA, we used morphological profiling of B.1.1.7 infected VeroE6 cells to
285 evaluate the effect of niclosamide treatment on SARS-CoV-2 infection. We found that
286 niclosamide inhibits the spread of virus to adjacent cells in a concentration-dependent fashion as
287 indicated by the reduction in size of viral syncytia. We also observed that the total number of
288 viral objects (individually infected cells or syncytia) decreased with niclosamide treatment,
289 which is consistent with entry inhibition. For example, if niclosamide were only influencing cell-
290 to-cell spread, the total number of viral objects would remain constant and only the size of the
291 syncytia would be affected. While the complete mechanism of action for niclosamide is
292 complex, our results suggest that both inhibition of cell-to-cell spread and entry inhibition play a
293 role in its activity (**Figure 6**). The degree to which each of the MOAs contributes to efficacy may
294 be different for SARS-CoV-2 variants, which could help explain the differences in potency.

295 The polypharmacology of niclosamide is a major issue for its utility as a COVID-19 antiviral.
296 Niclosamide is known to influence many different signal transduction pathways and has been
297 implicated in the treatment of a wide range of diseases including several cancers, bacterial
298 infections, viral infections, type 2 diabetes, non-alcoholic fatty liver disease, rheumatoid arthritis,
299 and others. Unfortunately, the mechanism of action for niclosamide remains elusive for the
300 majority of its biological effects. It is often unclear if there is a direct interaction between
301 niclosamide and a molecular target, or if there is an indirect mechanism of action at play[21]. An
302 underlying mechanism for its broad activity may be its ability to act as a protonophore, which

303 has many different downstream effects in cells including disruption of pH gradients,
304 mitochondrial uncoupling, and transcriptional modulation of various gene targets[21]. This
305 mechanistic ambiguity also translates to its antiviral efficacy. It is likely that the antiviral
306 activities of niclosamide (e.g., inhibition of entry, replication, and syncytia formation) are all
307 downstream consequences of its activity as a nonspecific protonophore since activity was lost
308 following removal of the hydroxyl group. If this is the case, then it may be challenging to
309 separate the undesired off-target effects from the antiviral effects. While our studies suggest that
310 niclosamide and other mitochondrial uncouplers demonstrate anti-SARS-CoV-2 efficacy, further
311 studies are warranted to determine if these mechanisms of action are unified by protonophore
312 activity.

313 While niclosamide is not an ideal candidate itself, it may represent a promising chemical tool for
314 the development of more specific SARS-CoV-2 inhibitors. In particular, inhibition of cell-to-cell
315 spread by syncytia is an extremely attractive mechanism for inhibition. Syncytia, which are
316 multinucleated bodies resulting from the fusion of adjacent cells, are a key characteristic of
317 SARS-CoV-2 infection and have been observed in many post-mortem histological samples from
318 fatal COVID-19 cases[28,50]. Syncytia formation facilitates the rapid spread of the viral genome
319 between cells[51], which increases the area of infected tissue and may enhance immune system
320 evasion[52]. An inhibitor of cell-to-cell infection like niclosamide may be clinically useful for the
321 treatment or prevention of COVID-19, especially when cocktailed with other direct acting
322 antivirals.

323 In this study, we also tested the antiviral efficacy of 33 structural analogs of niclosamide to
324 establish a preliminary structure-activity relationship profile which could aid in the development
325 of compounds with antiviral efficacy and less off-target effects. We identified eight compounds

326 (compounds 2, 3, 4, 10, 11, 22, 24, 34) that were efficacious in both VeroE6 and H1437 cell
327 models and four of which had improved potency and reduced cytotoxicity in VeroE6
328 (Compounds 2,7,11 and 24). Consequently, we believe there is a potential for designing better
329 niclosamide analogs with improved properties. Additionally, our structure-activity analysis
330 revealed some mechanistic features of niclosamide. Most noteworthy, the removal of the
331 protonophore hydroxyl group resulted in complete loss of activity in both cell models. The
332 efficacy of analogs strongly relied on their weakly acidic and lipophilic nature. Analogs with
333 higher predicted acidity (pKa) due to the presence of carboxylic acid substituents were generally
334 completely inactive. We also determined that other protonophores, including FCCP and
335 oxyclozanide, also had anti-SARS-CoV-2 efficacy, suggesting that the ability to disrupt pH
336 gradients is central to the mechanism of action for niclosamide. Niclosamide has been shown to
337 neutralize endo-lysosomal pH gradients, which is believed to be responsible for its broad-
338 spectrum antiviral activity[24]. Our results indicate that this nonspecific mechanism of action also
339 significantly contributes to the activity of niclosamide against SARS-CoV-2.

340 Overall, the poor selectivity index, low bioavailability, complex polypharmacology, nonspecific
341 protonophore activity, and variant-dependent potency of niclosamide limit its potential as a
342 COVID-19 therapeutic. However, our studies have shown that changes to the salicyl and aniline
343 rings can modulate selectivity and bioavailability while maintaining its activity. Therefore,
344 niclosamide represents a useful chemical probe that can be leveraged in a large-scale SAR
345 campaign to design better analogs in the future.

346

347

348 **Methods**

349 **Compounds**

350 Niclosamide, FCCP, 2,4 DNP, Oxyclozanide and Dicumarol were obtained from Sigma Aldrich
351 and prepared as 10 mM stock solutions in dimethylsulfoxide (DMSO). The 33 structural analogs
352 of niclosamide were obtained from previous studies[38]. Compounds were solubilized at 10 mM in
353 DMSO, and were dispensed onto cells using an HPD300e digital compound dispenser.

354 **Cells and Virus**

355 VeroE6 cells were maintained in Dulbecco's Modified Eagle Medium (DMEM), and H1437 cells
356 were maintained in RPMI 1640 base medium. Both cell lines were supplemented with 10% fetal
357 bovine serum (FBS) and 1X pen-strep solution and were grown at 37°C with 5% CO_2 following
358 standard cell culture procedures. These cell lines were tested for mycoplasma contamination
359 before use and were negative. The following reagents were deposited by the Centers for Disease
360 Control and Prevention and were obtained through BEI resources, NIAID, NIH: SARS-Related
361 Coronavirus 2, Isolate USA-WA1/2020, NR-52281, USA/CA_CDC_5574/2020 (B.1.1.7), NR-
362 54011, USA/MD-HP01542/2021 (Lineage B.1.351), NR-55282, Japan/TY7-503/2021 (Brazil
363 P.1), NR-54982, USA/PHC658/2021 (Lineage B.1.617.2), NR-55611.Viral stocks were grown in
364 VeroE6 and titers were determined by TCID50 using the Reed and Muench method[53]. All the
365 work with live SARS-CoV-2 virus was performed in biosafety level-3 containment lab (BSL3)
366 with the approval of the University of Michigan's Department of Environment and Health and
367 Safety and the Institutional Biosafety Committee.

368

369 **Anti-SARS-CoV-2 high content bioassays**

370 Assays were adapted from previous work and optimized for H1437 and VeroE6 cell lines[17,54].
371 For 48-hour infection experiments, VeroE6 and H1437 cells were seeded onto 384 well plates
372 (6057300, Perkin Elmer) at densities of 3000 and 5000 cells per well, respectively, in 50 µL of
373 media. After 24 hours of cell attachment at 37°C and 5% CO_2, compounds were dispensed
374 directly to the cell plates using an HPD300e digital compound dispenser. All wells were
375 normalized to a constant DMSO concentration of 0.2%, and plates contained both infected and
376 uninfected control wells. After 24 hours of preincubation with compounds, cells were inoculated
377 with the indicated SARS-CoV-2 variant at MOIs of 0.1 for VeroE6 and 1 for H1437. Cells were
378 incubated with virus and compounds for an additional 48 hours and then fixed with 4%
379 paraformaldehyde for 30 minutes at room temperature. Cells were then permeabilized with 0.3%
380 Triton-X100 for 15 minutes and stained with anti-nucleocapsid protein primary antibody
381 (ABIN6952432, Antibodies Online) at a dilution of 1:2000 overnight at +4°C. Following
382 primary antibody staining, cells were stained with a dye cocktail containing 1:1000 secondary
383 antibody Alexa-647 (goat anti-mouse, A21235, Thermo Fisher) and 10 µg/mL Hoechst 33342
384 pentahydrate (bis-benzimide) for nuclear labeling for a total of 30 minutes at room temperature.
385 Cells were stored in PBS before imaging. For 24-hour infection experiments, the methods were
386 comparable except that VeroE6 cells were seeded at 5000 cells per well, compounds were
387 preincubated for 1 hour instead of 24, and the infection window was 24 hours instead of 48. All
388 other inoculation, fixation and staining procedures were identical.

389 **High Content Imaging**

390 Stained assay plates were imaged using a both a Thermo Fisher CX5 with a 10X/0.45NA
391 objective lens and a Yokogawa Cell Voyager 8000 (CV8000) microscope with a 20X/1.0NA

392 water immersion lens. Imaging techniques were followed as described previously for detection
393 of nuclei and SARS-CoV-2 nucleocapsid protein[17,54]. A total of N=9 fields per well were imaged
394 for all assay plates, accounting for roughly 80% of the total well area.

395 **Image Processing**

396 Images were processed using the image segmentation and analysis software CellProfiler 4.0[55].
397 Separate pipelines were developed for H1437 and VeroE6 images. Pipelines were used to
398 identify nuclei (Hoechst 33342) and viral objects including multinucleated syncytia and
399 individually infected cells (Alexa Fluor 647) by adaptive otsu thresholding. Similar to previous
400 work, infected cells were identified using the *relateobjects* module whereby any nucleus
401 contained within a viral object was defined as infected[54]. For morphological profiling of B.1.1.7
402 infection vs. niclosamide in VeroE6, additional intensity, textural and spatial features were
403 measured using CellProfiler 4.0 for both the nuclear and viral channels.

404 **Concentration response analysis and IC_{50}/CC_{50} determination**

405 Field level data were grouped at the well level using Knime[56] and used to determine normalized
406 percent infection and percent viability scores. Raw percent infection per well was determined by
407 taking the ratio of infected nuclei to total nuclei and multiplying by 100. Normalized percent
408 infection was then generated such that "100% infection" was equivalent to the average raw
409 percent infection of the viral control for each plate. Cell counts for the entire plate were
410 normalized and 100% viability was based on the average cell count of the infected DMSO
411 control wells. Concentration-response curves were plotted in GraphPad Prism 9.0 (GraphPad
412 Software) and fitted using a semi-log 4-parameter variable slope model. IC_{50} and CC_{50} values were
413 extracted from percent infection curves and percent viability curves, respectively. Selectivity
414 indices were determined by taking a ratio of the CC_{50} and IC_{50}.

415 **High content imaging analysis of B.1.1.7 infection versus niclosamide**

416 Object level data for nuclei and viral objects (syncytia and individually infected cells) was used
417 to evaluate morphological and phenotypic features of B.1.1.7 infection versus niclosamide
418 including changes in N protein intensity and area of viral objects. Only images for the infected
419 DMSO vehicle control, as well as 3 different concentrations of niclosamide (156 nM, 313 nM
420 and 625 nM) were included in this analysis. The max viral object area reported in Figure 3A
421 represents the largest viral object observed for each condition including all fields and replicate
422 wells. The mean N protein intensity for infected cells was computed at the object level and the
423 results from Figure 3C include data for cells in each condition.

424 **Statistical analysis and hypothesis testing**

425 All statistical analyses and hypothesis testing was performed using GraphPad Prism 9.0
426 (GraphPad software). Specifics for statistical analyses, including sample sizes and other
427 important data are included within the text of figure legends.

428 **Acknowledgements**

429 We acknowledge funding from the University of Michigan Institute for Clinical and Health
430 Research (MICHR; National Center for Advancing Translational Science Grant UL1TR002240)
431 and the U-M Center for Drug Repurposing. JZS is supported by the National Institute of
432 Diabetes and Kidney Diseases (R01DK120623). CEW is supported in part by The University of
433 Michigan Biological Scholars Science Program. JWW is supported by an American Foundation
434 for Pharmaceutical Education (AFPE) regional award. CM is supported by European funding
435 MSCA actions, GA481247. SRM is supported by a pharmacological sciences training program
436 (PSTP) T32 training grant. We thank Tracey Schultz for thoughtful discussions and assistance

437 with cell culture. Figures were generated using Biorender.com. The authors declare no conflicts

438 of interest.

439 **References**

440 1. Hu, B., Guo, H., Zhou, P. & Shi, Z. L. Characteristics of SARS-CoV-2 and COVID-19. *Nature Reviews*
441 *Microbiology 2020 19:3* **19**, 141–154 (2020).

442 2. Aslan, A., Aslan, C., Zolbanin, N. M. & Jafari, R. Acute respiratory distress syndrome in COVID-19:
443 possible mechanisms and therapeutic management. *Pneumonia 2021 13:1* **13**, 1–15 (2021).

444 3. Mizrahi, B. *et al.* Longitudinal symptom dynamics of COVID-19 infection. *Nature Communications*
445 *2020 11:1* **11**, 1–10 (2020).

446 4. Dong, E., Du, H. & Gardner, L. An interactive web-based dashboard to track COVID-19 in real
447 time. *Lancet Infect Dis* **20**, 533–534 (2020).

448 5. Harvey, W. T. *et al.* SARS-CoV-2 variants, spike mutations and immune escape. *Nat Rev Microbiol*
449 **19**, 409–424 (2021).

450 6. Kyriakidis, N. C., López-Cortés, A., González, E. V., Grimaldos, A. B. & Prado, E. O. SARS-CoV-2
451 vaccines strategies: a comprehensive review of phase 3 candidates. *npj Vaccines 2021 6:1* **6**, 1–17
452 (2021).

453 7. Cully, M. A tale of two antiviral targets - and the COVID-19 drugs that bind them. *Nat Rev Drug*
454 *Discov* **21**, 3–5 (2022).

455 8. Whitley, R. Molnupiravir — A Step toward Orally Bioavailable Therapies for Covid-19. *New*
456 *England Journal of Medicine* **386**, 592–593 (2022).

457 9. Hammond, J. *et al.* Oral Nirmatrelvir for High-Risk, Nonhospitalized Adults with Covid-19. *New*
458 *England Journal of Medicine* **386**, 1397–1408 (2022).

459 10. Feinmann, J. Covid-19: global vaccine production is a mess and shortages are down to more than
460 just hoarding. *BMJ* **375**, (2021).

461 11. Qomara, W. F., Primanissa, D. N., Amalia, S. H., Purwadi, F. v. & Zakiyah, N. Effectiveness of
462 Remdesivir, Lopinavir/Ritonavir, and Favipiravir for COVID-19 Treatment: A Systematic Review.
463 *Int J Gen Med* **14**, 8557–8571 (2021).

464 12. Gottlieb, R. L. *et al.* Early Remdesivir to Prevent Progression to Severe Covid-19 in Outpatients. *N*
465 *Engl J Med* **386**, 305–315 (2022).

466 13. Chen, R. E. *et al.* Resistance of SARS-CoV-2 variants to neutralization by monoclonal and serum-
467 derived polyclonal antibodies. *Nature Medicine 2021 27:4* **27**, 717–726 (2021).

468 14. Takashita, E. *et al.* Efficacy of Antiviral Agents against the SARS-CoV-2 Omicron Subvariant BA.2.
469 *New England Journal of Medicine* **386**, 1475–1477 (2022).

470 15. Pushpakom, S. *et al.* Drug repurposing: progress, challenges and recommendations. *Nature*
471 *Reviews Drug Discovery 2018 18:1* **18**, 41–58 (2018).

472 16. Drayman, N. *et al.* Masitinib is a broad coronavirus 3CL inhibitor that blocks replication of SARS-
473 CoV-2. *Science (1979)* **373**, 931–936 (2021).

474 17. Mirabelli, C. *et al.* Morphological cell profiling of SARS-CoV-2 infection identifies drug repurposing
475 candidates for COVID-19. *Proc Natl Acad Sci U S A* **118**, (2021).

476 18. Touret, F. *et al.* In vitro screening of a FDA approved chemical library reveals potential inhibitors
477 of SARS-CoV-2 replication. *Scientific Reports* **10**, 13093 (2020).

478 19. Xiao, X. *et al.* Identification of Potent and Safe Antiviral Therapeutic Candidates Against SARS-
479 CoV-2. *Frontiers in Immunology* **11**, (2020).

480 20. Jeon, S. *et al.* Identification of antiviral drug candidates against SARS-CoV-2 from FDA-approved
481 drugs. *Antimicrobial Agents and Chemotherapy* **64**, (2020).

482 21. Chen, W., Mook, R. A., Premont, R. T. & Wang, J. Niclosamide: Beyond an antihelminthic drug.
483 *Cellular Signalling* **41**, 89–96 (2018).

484 22. Fonseca, B. D. *et al.* Structure-activity analysis of niclosamide reveals potential role for
485 cytoplasmic pH in control of mammalian target of rapamycin complex 1 (mTORC1) signaling. *J*
486 *Biol Chem* **287**, 17530–17545 (2012).

487 23. Kumar, R. *et al.* Mitochondrial uncoupling reveals a novel therapeutic opportunity for p53-
488 defective cancers. *Nature Communications 2018 9:1* **9**, 1–13 (2018).

489 24. Jurgeit, A. *et al.* Niclosamide Is a Proton Carrier and Targets Acidic Endosomes with Broad
490 Antiviral Effects. *PLoS Pathogens* **8**, 1002976 (2012).

491 25. Wu, C. J. *et al.* Inhibition of Severe Acute Respiratory Syndrome Coronavirus Replication by
492 Niclosamide. *Antimicrobial Agents and Chemotherapy* **48**, 2693 (2004).

493 26. Prabhakara, C. *et al.* Strategies to target SARS-CoV-2 entry and infection using dual mechanisms
494 of inhibition by acidification inhibitors. *PLOS Pathogens* **17**, e1009706 (2021).

495 27. Gassen, N. C. *et al.* SARS-CoV-2-mediated dysregulation of metabolism and autophagy uncovers
496 host-targeting antivirals. *Nature Communications 2021 12:1* **12**, 1–15 (2021).

497 28. Braga, L. *et al.* Drugs that inhibit TMEM16 proteins block SARS-CoV-2 spike-induced syncytia.
498 *Nature 2021 594:7861* **594**, 88–93 (2021).

499 29. Lin, C. K. *et al.* Preclinical evaluation of a nanoformulated antihelminthic, niclosamide, in ovarian
500 cancer. *Oncotarget* **7**, 8993 (2016).

501 30. Fan, X., Li, H., Ding, X. & Zhang, Q. Y. Contributions of Hepatic and Intestinal Metabolism to the
502 Disposition of Niclosamide, a Repurposed Drug with Poor Bioavailability. *Drug Metab Dispos* **47**,
503 756–763 (2019).

504 31. Chang, Y. W. *et al.* Pharmacokinetics of anti-SARS-CoV agent niclosamide and its analogs in rats.
505 *Journal of Food and Drug Analysis* **14**, 15 (2020).

506 32. Reddy, A. S. & Zhang, S. Polypharmacology: drug discovery for the future. *Expert Rev Clin*
507 *Pharmacol* **6**, 41–47 (2013).

508 33. Wieland, A. *et al.* Anticancer effects of niclosamide in human glioblastoma. *Clin Cancer Res* **19**,
509 4124–4136 (2013).

510 34. Hamdoun, S., Jung, P. & Efferth, T. Drug repurposing of the anthelmintic niclosamide to treat
511 multidrug-resistant leukemia. *Frontiers in Pharmacology* **8**, (2017).

512 35. Rajah, M. M. *et al.* SARS-CoV-2 Alpha, Beta, and Delta variants display enhanced Spike-mediated
513 syncytia formation. *EMBO J* **40**, (2021).

514 36. Saito, A. *et al.* Enhanced fusogenicity and pathogenicity of SARS-CoV-2 Delta P681R mutation.
515 *Nature* **602**, 300–306 (2022).

516 37. Zhang, Y. *et al.* SARS-CoV-2 spike L452R mutation increases Omicron variant fusogenicity and
517 infectivity as well as host glycolysis. *Signal Transduction and Targeted Therapy 2022 7:1* **7**, 1–3
518 (2022).

519 38. Bhagat, H. A. *et al.* N-substituted phenylbenzamides of the niclosamide chemotype attenuate
520 obesity related changes in high fat diet fed mice. *PLOS ONE* **13**, e0204605 (2018).

521 39. Park, K. S. *et al.* FCCP depolarizes plasma membrane potential by activating proton and Na+
522 currents in bovine aortic endothelial cells. *Pflugers Archiv : European journal of physiology* **443**,
523 344–352 (2002).

524 40. Blaikie, F. H. *et al.* Targeting dinitrophenol to mitochondria: limitations to the development of a
525 self-limiting mitochondrial protonophore. *Biosci Rep* **26**, 231–243 (2006).

526 41. Shrestha, R., Johnson, E. & Byrne, F. L. Exploring the therapeutic potential of mitochondrial
527 uncouplers in cancer. *Molecular Metabolism* **51**, 101222 (2021).

528 42. Kotova, E. A. & Antonenko, Y. N. Fifty Years of Research on Protonophores: Mitochondrial
529 Uncoupling As a Basis for Therapeutic Action. *Acta Naturae* **14**, 4 (2022).

530 43. Blake, S. *et al.* Salicylanilides Reduce SARS-CoV-2 Replication and Suppress Induction of
531 Inflammatory Cytokines in a Rodent Model. *ACS Infectious Diseases* **7**, 2229–2237 (2021).

532 44. Cairns, D. M. *et al.* Efficacy of Niclosamide vs Placebo in SARS-CoV-2 Respiratory Viral Clearance,
533 Viral Shedding, and Duration of Symptoms Among Patients With Mild to Moderate COVID-19: A
534 Phase 2 Randomized Clinical Trial. *JAMA Network Open* **5**, e2144942–e2144942 (2022).

535 45. Parikh, M. *et al.* Phase Ib trial of reformulated niclosamide with abiraterone/prednisone in men
536 with castration-resistant prostate cancer. *Scientific Reports 2021 11:1* **11**, 1–7 (2021).

537 46. Lin, C. K. *et al.* Preclinical evaluation of a nanoformulated antihelminthic, niclosamide, in ovarian
538 cancer. *Oncotarget* **7**, 8993 (2016).

539 47. Backer, V. *et al.* A randomized, double-blind, placebo-controlled phase 1 trial of inhaled and
540 intranasal niclosamide: A broad spectrum antiviral candidate for treatment of COVID-19. *The*
541 *Lancet Regional Health - Europe* **4**, 100084 (2021).

542 48. Liu, H., Wei, P., Kappler, J. W., Marrack, P. & Zhang, G. SARS-CoV-2 Variants of Concern and
543 Variants of Interest Receptor Binding Domain Mutations and Virus Infectivity. *Frontiers in*
544 *Immunology* **13**, 50 (2022).

545 49. Weiss, A. *et al.* Niclosamide shows strong antiviral activity in a human airway model of SARS-CoV-
546 2 infection and a conserved potency against the Alpha (B.1.1.7), Beta (B.1.351) and Delta variant
547 (B.1.617.2). *PLOS ONE* **16**, e0260958 (2021).

548 50. Bussani, R. *et al.* Persistence of viral RNA, pneumocyte syncytia and thrombosis are hallmarks of
549 advanced COVID-19 pathology. *EBioMedicine* **61**, (2020).

550 51. Lin, L., Li, Q., Wang, Y. & Shi, Y. Syncytia formation during SARS-CoV-2 lung infection: a disastrous
551 unity to eliminate lymphocytes. *Cell Death & Differentiation 2021 28:6* **28**, 2019–2021 (2021).

552 52. Rajah, M. M., Bernier, A., Buchrieser, J. & Schwartz, O. The Mechanism and Consequences of
553 SARS-CoV-2 Spike-Mediated Fusion and Syncytia Formation. *Journal of Molecular Biology* **434**,
554 167280 (2022).

555 53. Reed, L. J. & Muench, H. A simple method of estimating fifty per cent endpoints. *American*
556 *Journal of Epidemiology* **27**, 493–497 (1938).

557 54. Wotring, J. W., Fursmidt, R., Ward, L. & Sexton, J. Z. Evaluating the in vitro efficacy of bovine
558 lactoferrin products against SARS-CoV-2 variants of concern. *J Dairy Sci* **105**, 2791–2802 (2022).

559 55. McQuin, C. *et al.* CellProfiler 3.0: Next-generation image processing for biology. *PLOS Biology* **16**,
560 e2005970 (2018).

561 56. Berthold, M. R. *et al.* KNIME - the Konstanz information miner. *ACM SIGKDD Explorations*
562 *Newsletter* 58–61 (2009) doi:10.1145/1656274.1656280.

563

564

565

566

567

568

569

570

571

572

573 **Figures**

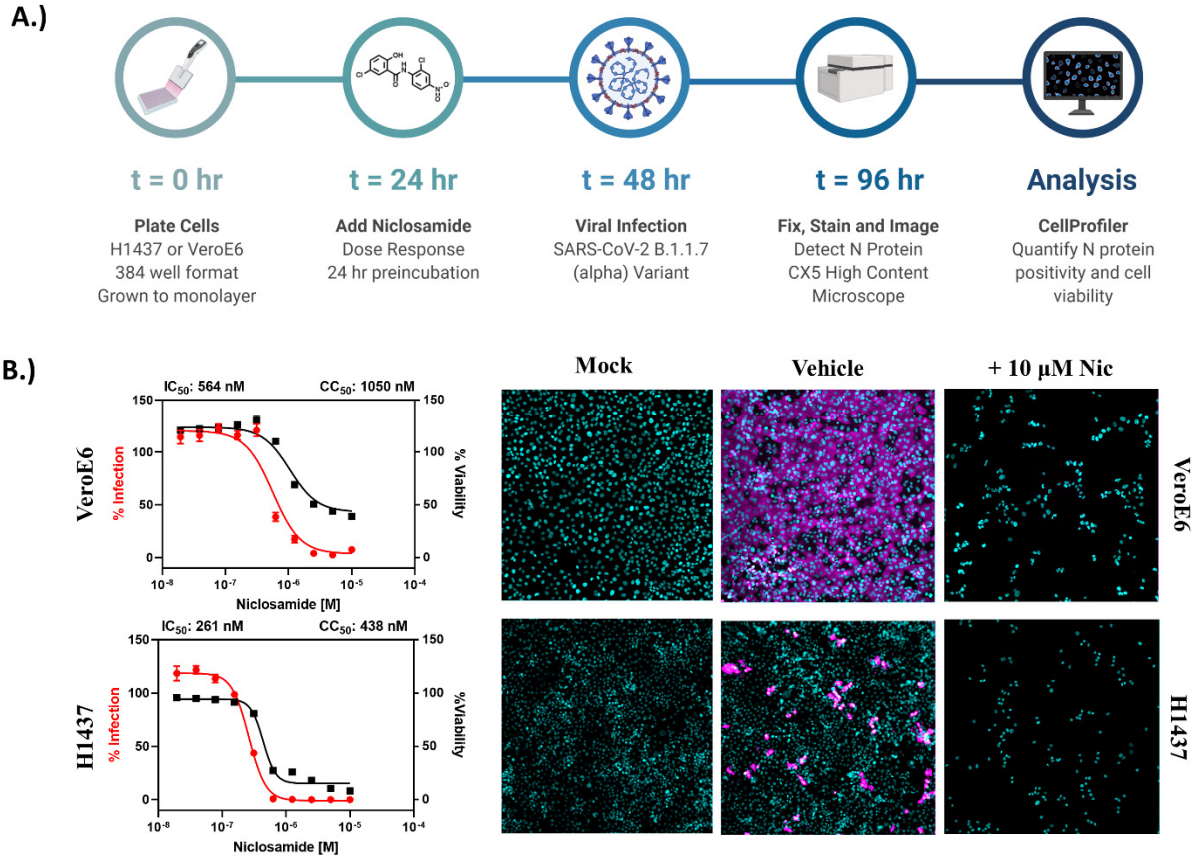

574

575 **Figure 1. Niclosamide is toxic at antiviral concentrations after long term exposure.** A.)
576 Workflow for high content anti-SARS-CoV-2 bioassay screening to determine infection
577 inhibition and cytotoxicity. B.) 10-point, 2-fold dilution concentration-response curves for
578 VeroE6 and H1437 cells with a starting concentration of 10 µM. VeroE6 cells were infected with
579 SARS-CoV-2 B.1.1.7 variant at a multiplicity of infection (MOI) of 0.1, while H1437 were
580 infected with SARS-CoV-2 WA1 variant at an MOI =1 to achieve optimal infection at 48 hours
581 post-infection. Data points represent mean ± SEM for N=10 replicates per condition. Curve
582 fitting was performed in GraphPad Prism 9.0 using a semi-log 4-parameter variable slope model.
583 Representative overlay images for mock, vehicle, and 10 µM Niclosamide treatment (infected)
584 are included (cyan = nuclei, magenta = SARS-CoV-2 N protein).

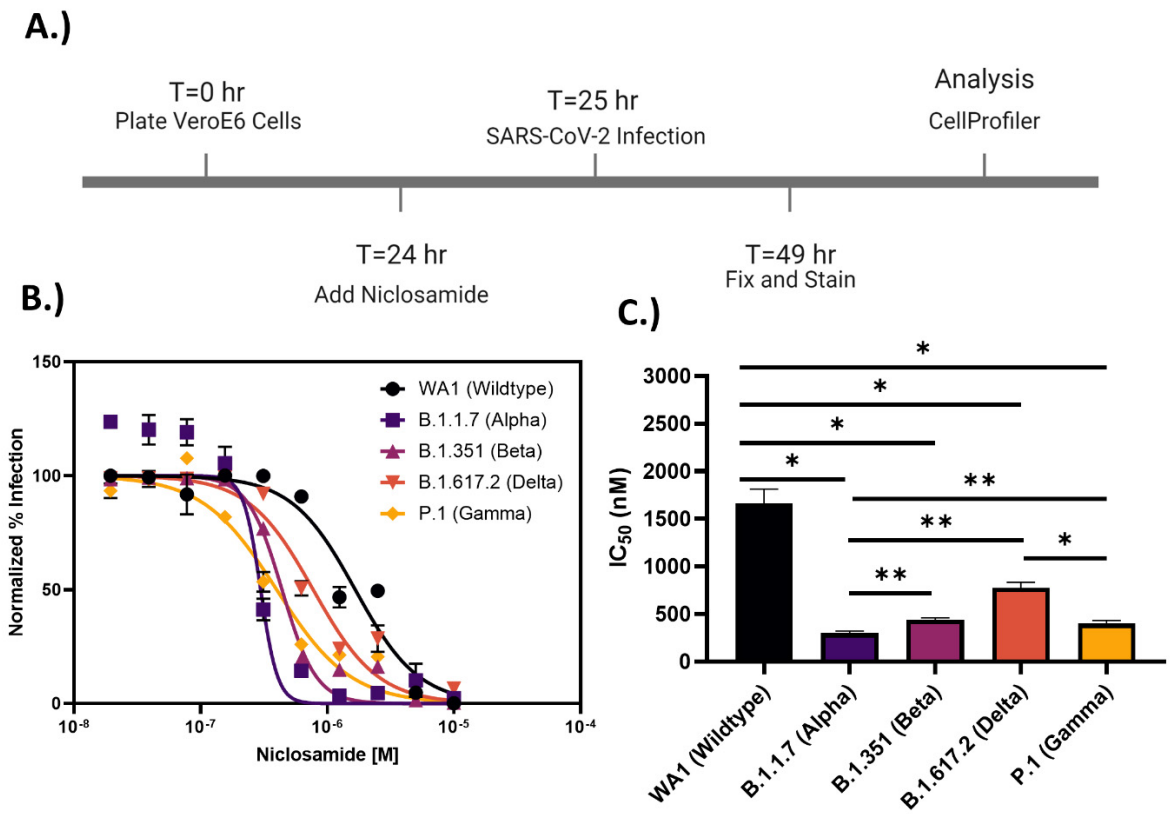

585

586 **Figure 2. Niclosamide potency is SARS-CoV-2 variant dependent.** A.) Assay timeline for
587 24-hour infection experiment. The assay window was shortened to reduce niclosamide toxicity.
588 B.) 10-point 2-fold concentration-response curves for niclosamide against the different SARS-
589 CoV-2 variants of concern (MOI = 0.1 for each variant) with a top concentration of 10µM.
590 Curves were fitted with GraphPad Prism 9.0 software using a semi-log 4-parameter variable
591 slope model. Data for each variant was normalized to the average percent infected of its
592 respective viral control. Data points represent mean ± SEM for N=3 replicates. C.) IC_{50} values
593 for niclosamide potency against SARS-CoV-2 variants of concern. Values were extracted from
594 curve fitting using GraphPad 9.0 and include SEM error bars (WA1: 1664 ± 149 nM, B.1.1.7:
595 298 ± 23 nM, B.1.351: 440 ± 21 nM, B.1.617.2: 774 ± 58 nM, P.1: 399 ± 34 nM). Significance
596 was determined using Student's T-tests (* = P<0.05, ** = P<0.01).

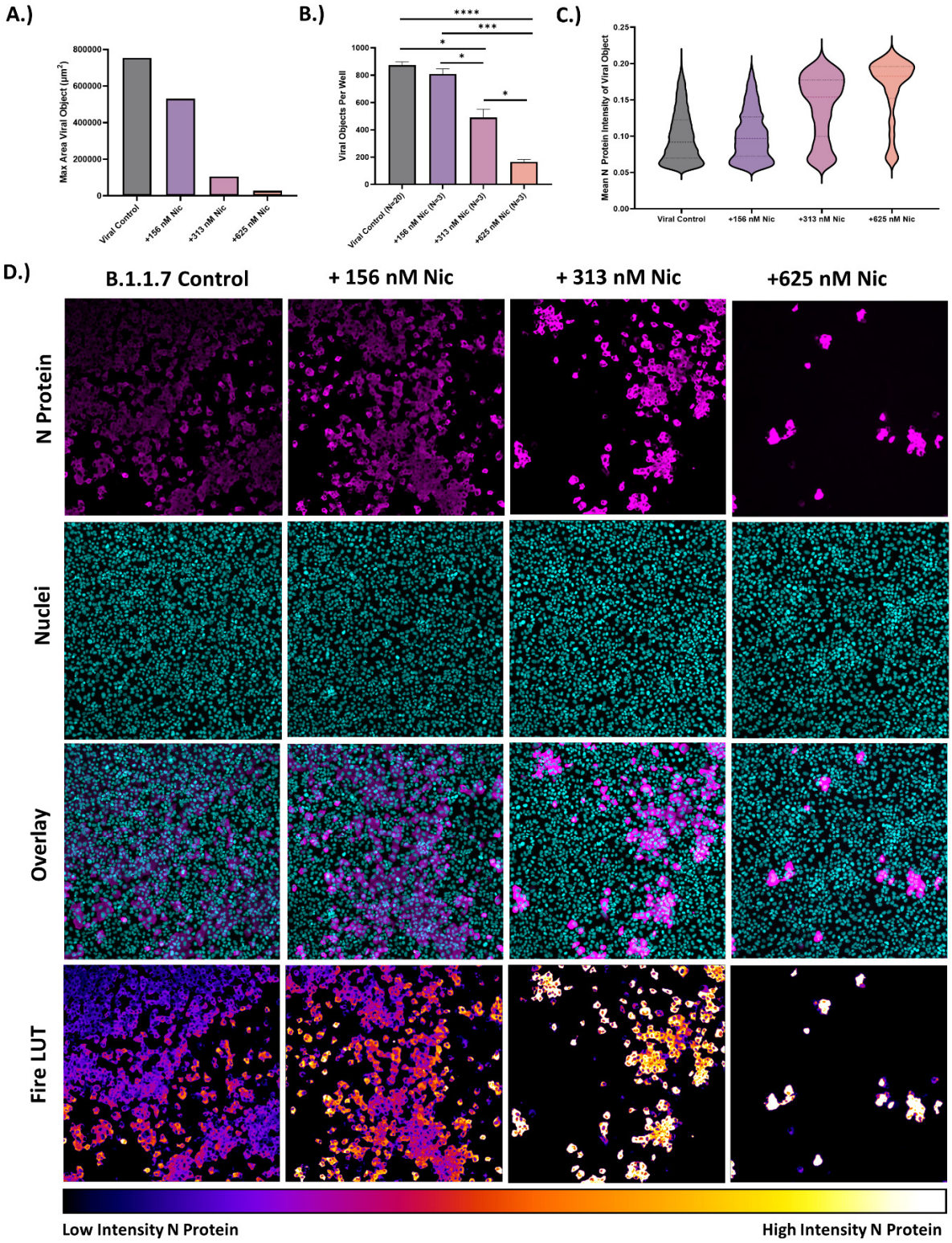
A.)
Max Area Viral Object (µm²)
800000
600000
400000
200000
0
Viral Control
+156 nM Nic
+313 nM Nic
+625 nM Nic
B.)
Viral Objects Per Well
1000
800
600
400
200
0
****
***
*
*
*
Viral Control (N=20)
+156 nM Nic (N=3)
+313 nM Nic (N=3)
+625 nM Nic (N=3)
C.)
Mean N Protein Intensity of Viral Object
0.25
0.20
0.15
0.10
0.05
0.00
Viral Control
+156 nM Nic
+313 nM Nic
+625 nM Nic
D.)
B.1.1.7 Control
+ 156 nM Nic
+ 313 nM Nic
+625 nM Nic
N Protein
Nuclei
Overlay
Fire LUT
Low Intensity N Protein
High Intensity N Protein

597

598

599 **Figure 3. Morphological profiling of B.1.1.7 infection versus niclosamide treatment in**
600 **VeroE6.** Image analysis reveals mechanistic characteristics of niclosamide activity against
601 SARS-CoV-2 infection. A.) The maximum area of viral objects decreases with increasing
602 niclosamide concentration. Data is the max area for viral objects in each condition. Viral control:
603 N=17452, +156 nM niclosamide: N=2425, +313 nM niclosamide: N= 1470, +625 nM
604 niclosamide: N= 496. B.) Viral objects per well decreases with increasing niclosamide
605 concentration. Viral objects include single infected cells and syncytia. Replicate values are
606 indicated on the X axis. C.) Mean pixel intensity for viral objects in each condition. Pixel
607 intensity increases with increasing niclosamide concentration. D.) Representative images for
608 each condition including N-protein channel, nuclear channel, an overlayed image and a fire
609 lookup table (LUT) image of the N-protein channel. Images were taken on a CX5 high content
610 microscope at 10X magnification. * = P<0.05, ***= P<0.001, ****= P<0.0001.

611
612
613
614
615
616
617
618
619
620
621
622
623
624

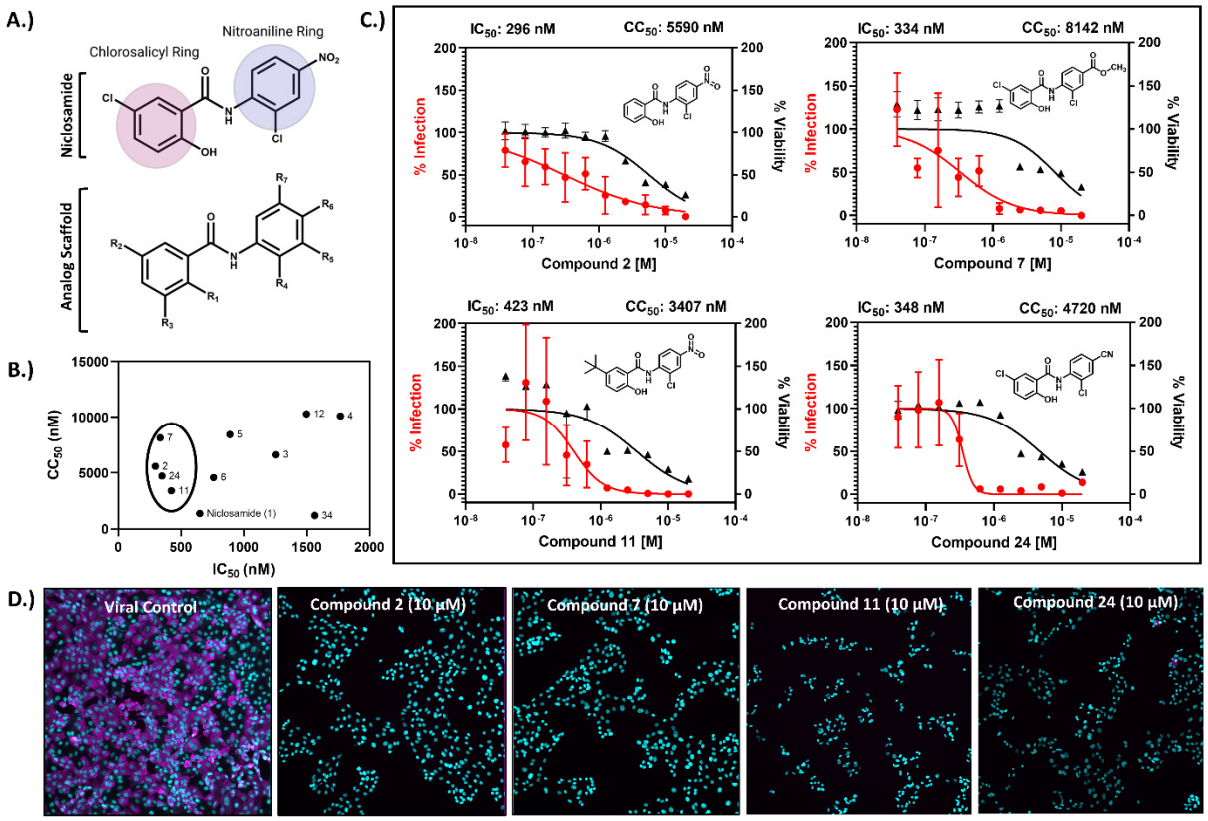

Figure 4. Niclosamide analogs have improved efficacy and reduced cytotoxicity in VeroE6. A.) Structure of niclosamide indicating the chlorosalicyl/nitroaniline rings, and analog scaffold with modified substituent positions labeled. B.) IC_{50} vs. CC_{50} plot highlighting efficacious compounds in VeroE6. Compounds with improved potency and cytotoxicity profiles are circled on the plot. C.) 10-point, 2-fold concentration-response curves for the top four niclosamide analogs with a starting concentration of 20µM. Data are shown as the mean ± SEM of N=3 replicate wells per condition. Curves for infection (in red) and cell viability (in black) are included. D.) Representative images of infected cells treated with indicated compounds and viral control (Vehicle). (10X magnification, Cyan = nuclei, magenta = SARS-CoV-2 nucleocapsid protein).

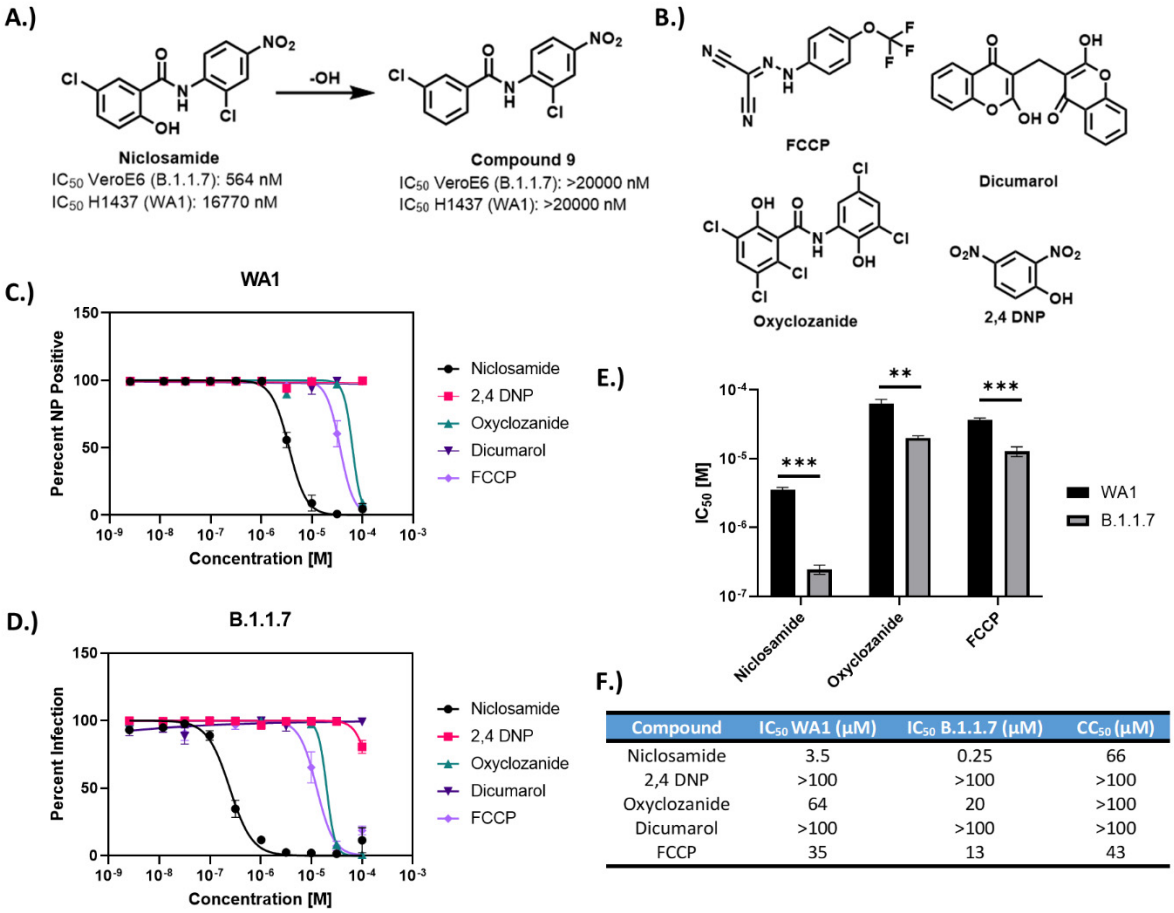

Compound	IC_{50} WA1 (μM)	IC_{50} B.1.1.7 (μM)	CC_{50} (μM)
Niclosamide	3.5	0.25	66
2,4 DNP	>100	>100	>100
Oxyclozanide	64	20	>100
Dicumarol	>100	>100	>100
FCCP	35	13	43

Figure 5. Efficacy of protonophores against SARS-CoV-2. A.) Removal of protonophore hydroxyl of niclosamide results in a complete loss of efficacy in both VeroE6 and H1437 cells. B.) Chemical structures for other protonophores evaluated against SARS-CoV-2 infection. C-D.) 10-point, 2-fold concentration response curves for protonophores versus WA1 variant (C.) and B.1.1.7 variant (D.) with starting concentrations of 100 μM. E.) IC_{50} plot for antiviral protonophores indicating significantly different potency against variants. F.) Table of IC_{50} and CC_{50} values for protonophores.

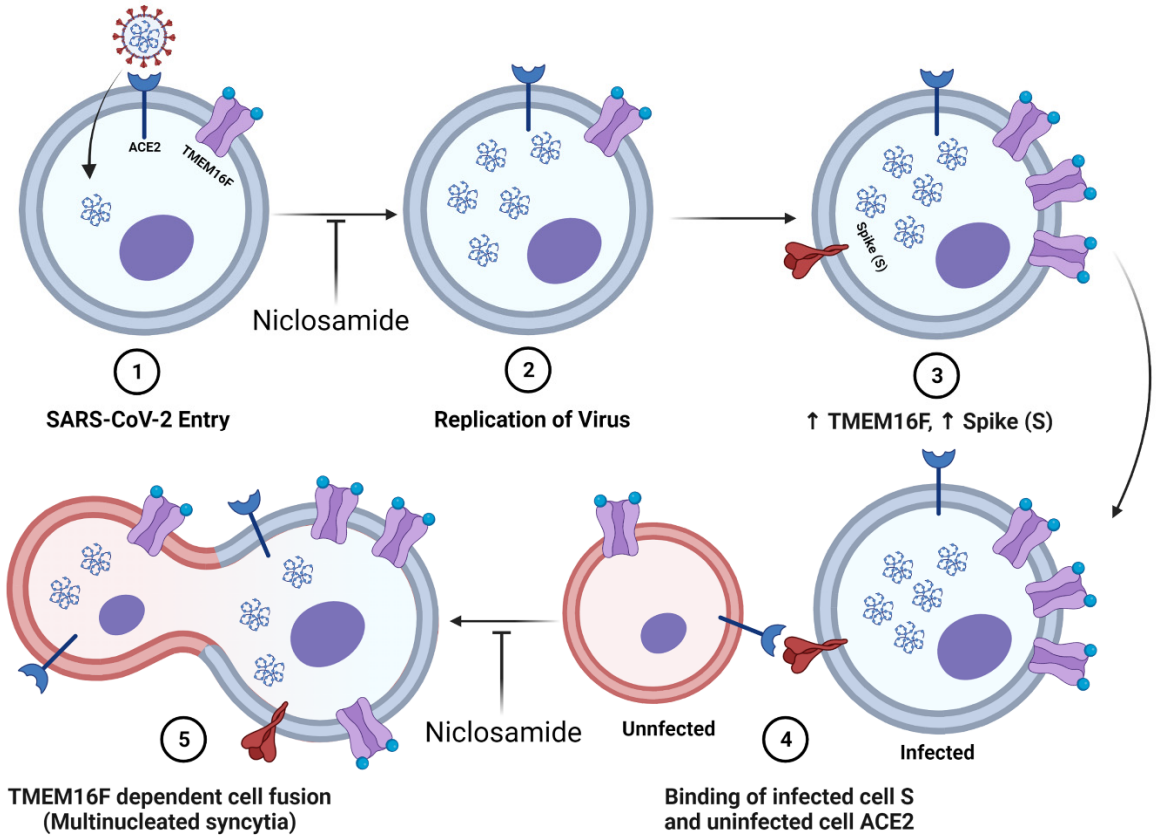

Figure 6. Diagram of niclosamides effect on SARS-CoV-2 entry and spike protein-mediated syncytia formation. 1.) SARS-CoV-2 binds to the ACE2 receptor of the host cell and enters. Niclosamide has been shown to inhibit this entry step *in vitro* 2.) Viral replication generates many copies of the RNA genome. 3.) Infection results in an increased expression of viral spike (S) protein and host cell TMEM16F at the plasma membrane. 4.) The S protein at the surface on an infected cell binds to the ACE2 receptor of an adjacent uninfected cell. 5.) Spike-dependent syncytia formation is mediated by the calcium-dependent lipid scramblase TMEM16F to generate multinucleated infected cell bodies. Niclosamide, an inhibitor of TMEM16F, has been shown to block spike-dependent syncytia formation.

659 **Tables**

660 **Table 1. SAR table for Niclosamide Analogs.** IC_{50} and CC_{50} values for VeroE6 (SARS-CoV-2
661 B.1.1.7 variant) and H1437 (SARS-CoV-2 WA1 variant). Physical properties including cLogP,
662 pKa and logS were calculated using MOE and included in the table for each compound.
663 Compounds that have efficacy against both cell lines are highlighted in gray.

Compound #	R1	R2	R3	R4	R5	R6	R7	Vero-E6 (B.1.1.7)		H1437 (WA1)		cLogP	pKa	logS
								IC_{50} (nM)	CC_{50} (nM)	IC_{50} (nM)	CC_{50} (nM)			
1 (Niclosamide)	OH	Cl	H	Cl	H	NO2	H	564	1050	16770	17060	4.17	7.98	-5.00
2	OH	H	H	Cl	H	NO2	H	296	5590	4915	8403	3.47	7.52	-4.32
3	OH	CH3	H	Cl	H	NO2	H	1254	6277	2595	3056	3.97	7.52	-4.66
4	OH	OCH3	H	Cl	H	NO2	H	1769	10110	10880	8941	3.39	7.65	-4.39
5	OH	Cl	H	Cl	H	H	H	890	8435	>20000	>20000	4.17	8.01	-4.54
6	OH	Cl	H	Cl	H	CH3	H	760	4591	>20000	6048	4.66	8.01	-4.88
7	OH	Cl	H	Cl	H	COOCH3	H	334	8142	Inverted	>20000	4.15	7.98	-4.94
8	OH	Cl	H	Cl	H	COOH	H	>20000	>20000	Inverted	>20000	3.67	4.03	-4.54
9	H	Cl	H	Cl	H	NO2	H	>20000	>20000	>20000	>20000	4.63	14	-5.27
10	OH	Cl	H	Cl	H	OCH3	H	4248	>20000	3097	1921	4.05	8.02	-4.59
11	OH	t-Bu	H	Cl	H	NO2	H	423	3407	16880	7529	5.50	7.51	-5.68
12	OH	OCH3	H	Cl	H	NO2	H	1498	10290	Inverted	>20000	3.39	7.65	-4.39
13	OH	t-Bu	H	Cl	H	COOCH3	H	>20000	14570	Inverted	>20000	5.49	7.50	-5.62
14	OH	t-Bu	H	Cl	H	COOH	H	>20000	14250	Inverted	>20000	5.00	4.93	-5.22
15	OH	t-Bu	H	F	H	COOH	H	>20000	>20000	Inverted	>20000	4.41	4.73	-4.69
16	OH	t-Bu	H	CH3	H	COOH	H	>20000	>20000	Inverted	>20000	4.49	4.95	-4.74
17	OH	t-Bu	H	Cl	H	H	COOH	>20000	>20000	Inverted	>20000	5.00	4.93	-5.22
18	OH	t-Bu	t-Bu	Cl	H	CH3SO2N	H	>20000	>20000	Inverted	>20000	5.98	7.02	-6.39
19	OH	t-Bu	t-Bu	Cl	H	NH2	H	>20000	17590	Inverted	>20000	6.58	7.57	-6.14
20	OH	t-Bu	t-Bu	H	CH3	COOH	H	>20000	>20000	>20000	>20000	6.52	4.96	-6.10
21	OH	Cy	H	Cl	H	COOCH3	H	9910	>20000	>20000	>20000	5.96	7.50	-6.66
22	OH	Cy	H	Cl	H	COOH	H	4511	>20000	7700	>20000	5.48	4.93	-6.26
23	OH	CF3	H	CH3	H	COOCH3	H	>20000	>20000	>20000	>20000	4.97	7.49	-5.15
24	OH	Cl	H	Cl	H	CN	H	348	4720	1070	880	4.27	8.00	-5.03
25	OH	H	t-Bu	Cl	H	COOCH3	H	>20000	>20000	Inverted	>20000	5.22	7.52	-5.52
26	OH	t-Bu	t-Bu	Cl	H	COOH	H	>20000	>20000	>20000	>20000	6.77	4.93	-6.48
27	OH	t-Bu	t-Bu	Cl	H	COOCH3	H	16500	>20000	>20000	>20000	6.52	4.96	-6.10
28	OH	OCH3	H	CH3	H	COOH	H	>20000	>20000	Inverted	>20000	2.38	4.95	-3.46
29	OH	H	t-Bu	Cl	H	COOCH3	H	>20000	>20000	Inverted	>20000	5.22	7.52	-5.52
30	OH	H	t-Bu	Cl	H	COOH	H	>20000	>20000	>20000	>20000	4.74	4.93	-5.12
31	OH	H	t-Bu	Cl	H	NO2	H	>20000	7214	>20000	1110	5.24	7.52	-5.58
32	OH	H	t-Bu	Cl	H	NH2	H	>20000	>20000	>20000	>20000	4.55	7.58	-4.78
33	OH	H	t-Bu	Cl	H	NSO2CH3	H	2879	>20000	Inverted	>20000	3.95	7.03	-5.03
34	OH	Cl	H	Cl	H	Br	H	760	5473	4067	3242	4.97	8.01	-5.36

664